A Double Multiple Stream Tube (DMST) routine to identify efficient geometries of cross-flow tidal turbines in site assessment analyses

M. Pucci [1,*], S. Zanforlin[1], D. Bellafiore[2] and G. Umgiesser[2,3]

[1] Dipartimento di Ingegneria dell'Energia, dei Sistemi, del Territorio e delle Costruzioni (DESTEC), Scuola di Ingegneria, Università di Pisa, l.go Lazzarino 1, 56100 Pisa, Italy. Email: micol.pucci@phd.unipi.it, stefania.zanforlin@unipi.it

[2] Istituto di Scienze Marine (ISMAR) del Consiglio Nazionale delle Ricerche (CNR), Arsenale Tesa 104, Castello 2737/F, 30122 Venezia. Email: debora.bellafiore@ve.ismar.cnr.it, georg.umgiesser@ismar.cnr.it

[3] Marine Research Institute, Klaipėda University, Klaipėda, Lithuania

[*] Corresponding author: M. Pucci, micol.pucci@phd.unipi.it

ABSTRACT

A routine to predict the performance of cross-flow hydrokinetic turbines, based on the Blade Element Momentum theory, for site assessment purposes is here presented. The routine uses as input the flow data obtained with the open-source marine circulation code SHYFEM. The routine consists in a Double Multiple Stream Tube model making use of 1D flow simplifications for fast analyses. The dynamic stall sub-model and two original sub-models, implemented to include the effects of blade tip losses and the lateral deviation of streamlines approaching the turbine, have been validated versus results of 3D and 2D CFD simulations. As a case study, the tool is applied to an area of the northern Adriatic Sea in order to quickly identify locations with the highest hydrokinetic potential and, at the same time, to find the most efficient turbine aspect ratio and configuration (single or paired turbines) taking into account the bathymetric constraints. The results show that turbines, with short aspect ratio, and paired turbines (with the same overall frontal area of a single rotor) can give the best power outputs thanks to higher flow speeds available at the top of the water column and more favorable Reynolds number and distribution of tip speed ratios along the blade.

Keywords: tidal turbines; site assessment; DMST; dynamic stall; aspect ratio; tip losses.

NOMENCLATURE

A	Turbine's frontal area [m^2]
A_{layer}	Frontal area of a vertical layer [m^2]
B	Number of blades
c	Turbine's chord [m]
C_P	Power coefficient
f	Arctangent of the flow deviation angle
k	Ratio between local C_P and mid plane C_P
L	Blade's length [m]
P	Generated Power [W]
P_{av}	Average available power [W]
R	Turbine's radius [m]
U_{av}	Velocity profile related to the average power available [m s^{-1}]
U_∞	Free stream velocity [m s^{-1}]
ρ	Fluid density [kg m^{-3}]
σ	Solidity
ω	Turbine's rotational speed [rad s^{-1}]
AR	Aspect Ratio
BEM	Blade Element Momentum

CFD Computational Fluid Dynamics
CFT Cross Flow Turbine
DMST Double Multiple Stream Tube
HAT Horizontal Axis Turbine
LEV Leading Edge Vortex
TSR Tip Speed Ratio

1. INTRODUCTION

Tidal stream energy is considered one of the most promising renewable resources in Europe and offers important benefits over wind or wave energy, such as perfect predictability and the device invisibility. Horizontal axis turbines (HATs) or cross-flow turbines (CFTs), also named vertical axis turbines, can be adopted. The CFT concept has aroused a growing interest in the last decade, thanks to the higher construction simplicity and the ability to work independently of flow direction, compared to HAT. Moreover, the adoption of a floating platform to sustain the rotor can give the further advantage of setting generator and gearbox above the sea level without any penalization with respect to a bottom-fixed system. The platform motion just negligibly affects the energy output, since performance is still good in skewed flow (Orlandi *et al.* 2015). Conversely, CFTs are affected by low starting-torque and lower efficiency than HATs, both shortcomings in theory lessened by means of blade-pitching mechanisms (Chougule *et al.* 2014) at the cost of a more complicated overall system. However, the factual strength of CFTs compared to HATs, which would more than compensate for the lower efficiency of the single device, is the higher power density achievable in case of a multi-device cluster or farm, i.e. the possibility to generate more electrical energy from a sea limited area. To this end, two strategies can be put into practice. The first is to tightly place the devices: (a) by adopting pairs of closely-spaced counter-rotating turbines, that can exploit beneficial fluid dynamic interactions (Zanforlin 2018); (b) by shortening the distances between the arrays, since peculiar physical mechanisms allow a fast energy recovery in the wakes of CFTs (Kinzel *et al.* 2012). The second strategy is to design the turbine with a high aspect ratio, *AR*, defined as $L/(2R)$, where L is the blade length, and R is the turbine radius, as shown in Fig. 1.

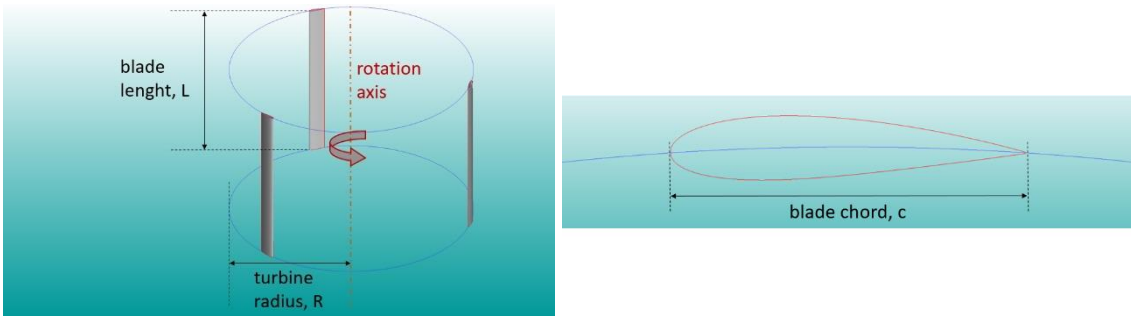

Figure 1. Turbine geometrical parameters (R, L, c).

Indeed, if the diameter of the turbine is fixed, an increase of *AR* implies a greater turbine cross-sectional area and then an enhanced power output. However, the blade length is not only limited by the bathymetric constraints but must consider the fluid dynamics phenomena induced by the presence of the turbine: the latter is only partially permeable to the incoming flow, and works as an obstacle generating a high momentum by-pass flow (Goward Brown *et al.* 2017). A proper distance between the blade tips and the free surface is useful to exploit the beneficial flow effects on the turbine output, and to allow the expansion and complete development of its wake (Birjandi *et al.* 2013; Kolekar *et al.* 2015). Whereas, an adequate blade tips distance from the seabed is necessary in order to avoid erosion, one of the greatest potential damages connected to marine turbine farms, since the generated by-pass flow increases the bed shear stress (Ramírez-Mendoza *et al.* 2020; Gillibrand *et al.* 2016). Furthermore, the choice of the blade length should also be guided by the real flow velocity vertical profile, since large velocity variations along the blade could imply a performance deterioration in extended regions of the blade. For all these reasons, site assessment tools should not disregard the geometric characteristics of the turbine. Coupling a 3D circulation code with a turbine analytical model based on the Blade-Element Momentum (BEM) theory is here proposed as the simplest approach. In case of

CFTs, the BEM approach consists in adopting a simplified aerodynamic analysis of the flow near the blade and solving momentum-balance equations across a single, multiple, or double-multiple stream-tube (DMST) passing through the turbine (Paraschivoiu 2002). To date, it is the most commonly used method to design the characteristics of the rotor, as hydrofoil shape, blade chord (c), number of blades (B), and optimal tip speed ratio (*TSR*), defined as $\omega R/U_\infty$, where ω is the turbine angular speed (in rad/s) and U_∞ is the free stream velocity. To identify the sites with the greatest potentials and the optimal turbine geometries to maximize the energy production, considering the real characteristics of the marine environment, the flow data coming from the marine code can be used as input for the BEM based model, since less computationally expensive and not requiring grid refinement (Deluca *et al.* 2018). In this paper we describe an easy methodology based on this kind of approach. Only after the turbine concept has already been inferred, the chosen turbine can be checked inside the marine code (Thiébot *et al.* 2020; Pucci *et al.* 2020). This will require very fine grids and long computation times, to assess the environmental impacts of a certain tidal farm layout.

2. METHODOLOGY

The turbine model has been developed at the University of Pisa. It consists in a DMST MATLAB routine, and uses the BEM theory in order to compute forces acting on blades, and then torque and power output, *P*. The structure of the DMST routine is detailed in (Deluca *et al.* 2018). The model allows predicting *P* as a function of the input variables, that are: lift and drag coefficients (depending on the blade profile, attack angle and Reynolds), *c*, number of blades, *R*, *AR*, freestream speed, *TSR*.

2.1 DMST sub-models

CFTs are characterized by not negligible unsteady effects as the dynamic stall. During the rotation of a blade, the angle of attack changes cyclically and significantly: the increase of the angle of attack lead to higher lift coefficient peaks, compared to those reached in static conditions. This effect is due to the development of the so called Leading Edge Vortex (LEV) near the hydrofoil. This vortex increases the suction on the hydrofoil preventing and delaying stall. For further increase of the angle of attack, LEV moves toward the trailing edge: this causes the drop of the lift force. These processes are reproduced through the dynamic stall model developed at the University of Pisa and thoroughly explained in (Rocchio *et al.* 2020). The model was adapted to the studied airfoil (NACA0018), since it originally was developed for another type.

Also flow curvature characterizes CFTs: although the flow can be approximated as straight, the composition of the flow motion direction with the turbine rotational motion, lead to a curved flow on the blade as explained in (Migliore *et al.* 1980). In order to avoid flow curvature effects, in this work CFD 2D and 3D models, used for the validation step, were set up with a supposed curved hydrofoil on a circumference with radius *R* (as shown in Fig. 1).

The model was implemented with a sub-model to represent the crosswise deviation of the streamlines belonging to the "streamtube" (i.e., the theoretical tube inside which the fluid passing through the rotor flows). As the turbine represents an obstacle to the incoming flow, the streamwise velocity is gradually decreased along the tube. Therefore, to satisfy the continuity equation, the crosswise section of the streamtube needs to widen and this also implies the fan-like widening of the streamlines. Moreover, the blade tip vortices entail additional crosswise velocity components that amplify the tube expansion. The streamlines deviation is observable both experimentally and by means of CFD simulations, yet the DMST model is a 1D model with straight streamlines unless we provide corrections. The correction we introduced is *TSR* dependent. Indeed, a higher *TSR* value corresponds to higher rotational speed, with consequent flow slowdown and increased deviation angle of the streamlines with respect to the direction of the undisturbed flow. It is like having a turbine less permeable to the flow. Solidity, σ, defined as $Bc/2\pi R$, also affects streamlines deviation, however all the analyses in this work were done by considering a three-bladed turbine with a fixed σ of 0.0637.

The implemented correction is based on CFD 2D simulations, carried out with the software ANSYS Fluent. The deviation angles were evaluated for different *TSR* at fixed azimuthal angles as shown in Fig. 2, where the flow moves from left to right.

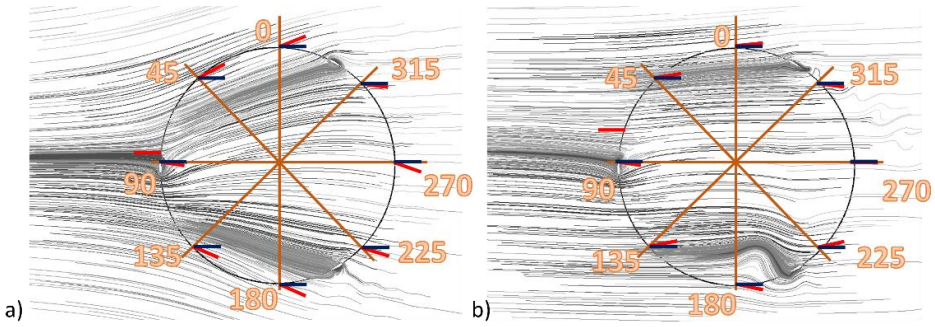

Figure 2. Flow deviation angles respect to the flow undisturbed direction at different TSR: a) 4; b) 1.2.

It is evident, that the flow deviation is more significant for higher *TSR* values. A correction formulation for the streamline deviation, was embedded in DMST model for both upstream and downstream tube (the half-left side and the half-right side of the turbine respectively in a top view). Flow deviation angles have been recorded for discretized values of azimuthal angle and *TSR*. Defining the *f* factor as the arctangent of the flow deviation angle, it is possible to evaluate the *f* factor for every *TSR* conditions, using interpolation.

The other phenomenon that must be considered are the fluid dynamic losses at the blade tips. According to the theory of finite wings, tip vortices are generated by the pressure difference between the pressure and the suction sides of any finite wing. Near the blade tip, the flow approaching the blade pressure-side is no longer able to follow the blade profile and curls around the tip towards the suction-side. The flow "leakage" around the tip decreases the pressure difference between the suction and pressure sides, as visible in Fig. 3a, thus reducing lift. Moreover, tip vortices imply a localized huge pressure drag increase. As a result, performance drastically drops at the blade tip (Zanforlin *et al.* 2018). The leakage is confirmed by Fig. 3b, showing streamlines departing from a line with the same height of the blade and set 1c upstream: it can be seen that part of the flow travelling across that line climbs over the tip. Since DMST model is a 1D model, it is important to introduce a correction for these 3D losses. Instead of the classical corrections by Prandtl-Glauert or Shen (2005), conceived for HATs and poorly considering the effects of *AR* and *TSR*, we based the correction on CFD 3D results. First of all, the power coefficient, C_P, i.e. the turbine fluid dynamic efficiency, has to be defined:

$$C_P = \frac{\mathrm{P}}{\frac{1}{2}\rho A U_\infty^2}, \tag{1}$$

where ρ is the water density and A is the frontal area. We have extracted the *k* factor, that represents the ratio between the local C_P along the blade and the C_P at the mid plane of the turbine. The *k* factor is equal to 1 at the mid plane of the turbine and decreases moving towards tips as shown in Fig. 4. CFD simulations were carried out at *TSR* 2.75 for two different *AR*: 2/3 and 2. Also in this case using interpolation we can obtain the *k* factor at every *z* positions along the blade and for every *AR* in the range mentioned above.

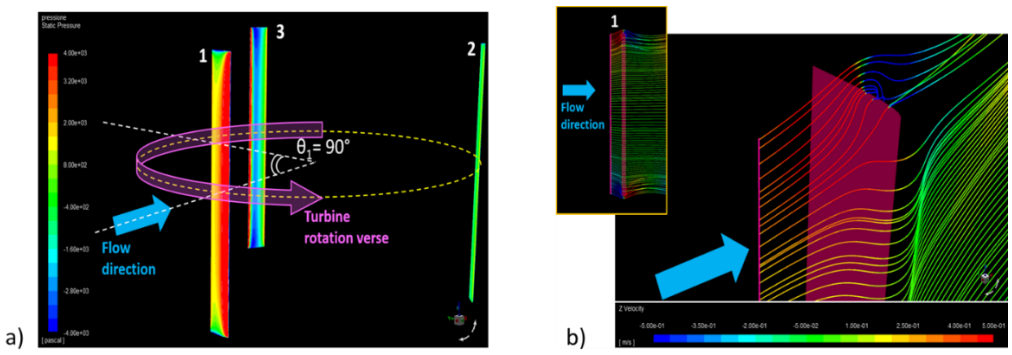

Figure 3. CFD results, *AR*=0.67 and *TSR*=2.77: a) static pressure on the blade surfaces for blade azimuthal angles: θ1 = 90°, θ2 = 210, θ3 = 330°; b) streamlines, starting from a segment placed 1c upstream the blade-1 (θ1 = 90°).

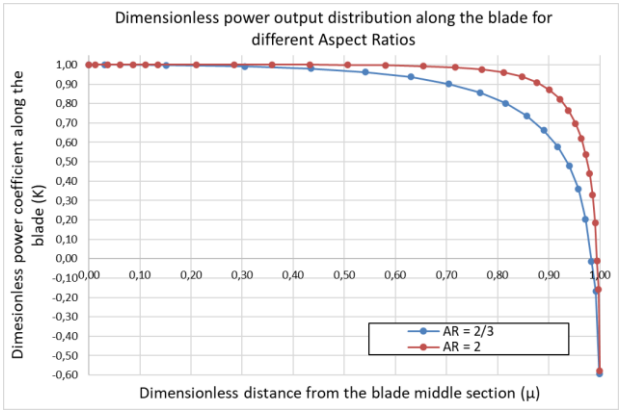

Figure 4. Trend of the *k* factor for 2 different *AR*: 2/3 and 2.

2.2 DMST calibration

In this work we have modified some sub-models embedded in the DMST to better represent the turbine we are interested in. For the dynamic stall sub-model, a tuning process was carried out until the behavior of the turbine matches with CFD 2-D results at different *TSR*. Fig. 5 shows the trend of turbine C_P compared to the one of CFD simulations. At low *TSR* (affected by stall conditions) the DMST curve steeply drops with respect to the CFD, whereas the optimum value of *TSR* (about 2.6) is a little over estimated.

For the simulations we have set the operating *TSR* at 2.77, higher than the optimal one. This *TSR* is used in the MATLAB DMST routine to calculate the rotational speed ω, assuming as reference undisturbed flow velocity the averaged velocity (weighted on the basis of power) along blade length.

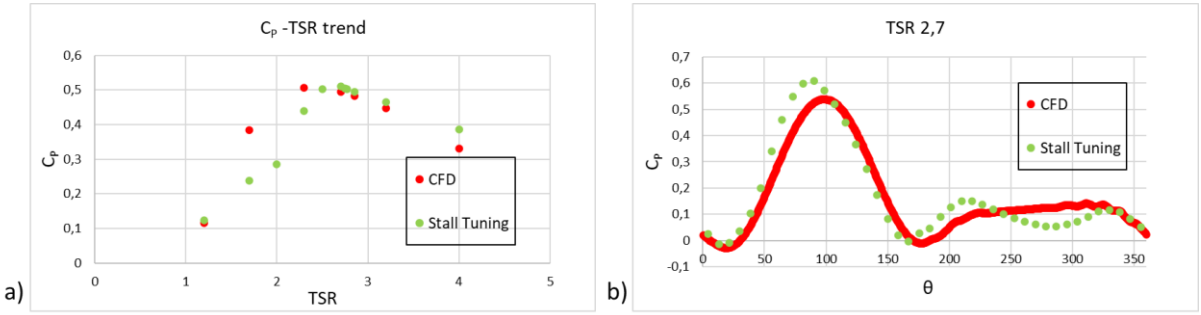

Figure 5. Comparison between CFD and DMST results, a) trend of C_P for different *TSR* and b) C_P for a single blade during rotation at *TSR* 2.7.

2.3 Coupling with SHYFEM for practical applications

The practical use proposed in this paper has the aim to identify suitable sites to place CFT, in order to choose those with the higher energy content and to establish the best turbine design to exploit the energy resource.

The area of study is located in the northern Adriatic Sea (latitude from 44.5 to 45.5 and longitude from 12 to 13). Flow data were achieved at CNR ISMAR of Venice by means of the SHYFEM 3D circulation code (Umgiesser *et al.* 2018), and cover a period from 7th to 21th of February 2014, hourly output (337 hours of simulation, about half lunar cycle). Results are computed vertically over 17 z layers, with increasing thickness (from 1 m at the surface to 2 m at the bottom). The horizontal discretization is about 600 m. Different turbine geometries have been tested. We had considered two values for the frontal area, and for each of them four values for the *AR*. Eight total combinations are analyzed, with different diameters, blade lengths and chord values, as shown in Fig. 6. Having set the σ at 0.063, larger diameters lead proportionally to higher chords.

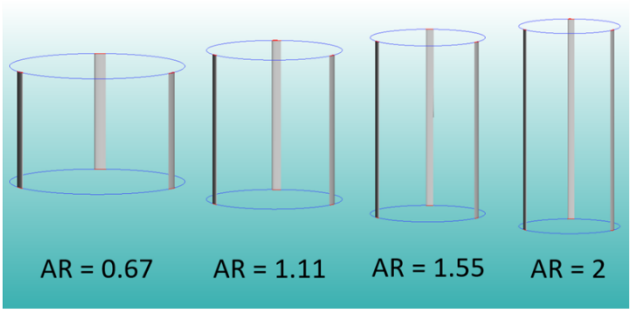

Area	AR	D [m]	H [m]	c [m]
25 m^2	0.67	6.1	4.1	0.41
	1.11	4.7	5.3	0.32
	1.55	4.0	6.2	0.27
	2	3.5	7.1	0.24
50 m^2	0.67	8.6	5.8	0.58
	1.11	6.7	7.5	0.45
	1.55	5.7	8.8	0.38
	2	5	10	0.33

Figure 6. Turbine geometric configurations compared in case study.

The first characterization of the area was based on the depth of the water column (Fig. 7a). A minimum distance of 2 m between the blades and the free surface, and between the blades and the seabed is assumed. It was necessary to exclude those sites where not even the smaller turbine could be installed due to the too shallow depth (black region in Fig. 7). Fig. 7b shows the power per unit area content of the upper layer (where flow speed is higher), in order to establish the location of major flow power.

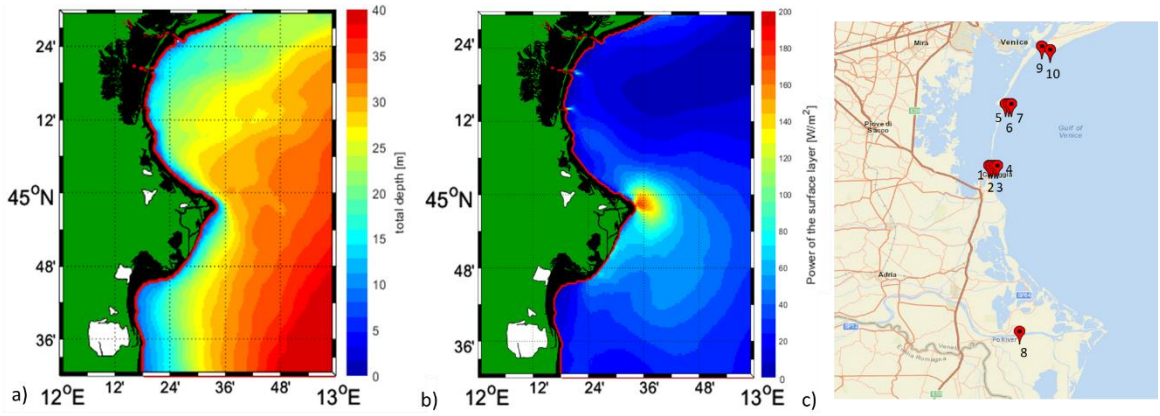

Figure 7. a) total depth of the seabed and b) power per unit area for the upper layer of the water column. The red line delimits areas where turbine can be placed from those where it can not. c) Map.

It can be observed that the power content is relevant in front of the Po River delta and at the three inlets connecting the lagoon to the Adriatic Sea. Suitable sites are identified where power available along blade is at least 50% of the maximum recorded power value. Computation is performed for each of the eight turbine cases. 10 sites have been identified (Fig. 7c). One suitable site is located along the main Po River branch, Pila.

We defined a methodology capable of comparing sites/geometries and evaluate energy production with a unique calculation by site and configuration, to avoid applying the routine to each of the 337 data series available. For this reason, we have estimated a reference velocity profile starting from the available averaged power in time as follows:

$$\mathrm{P_{av}}(z) = \frac{\sum_i^{time} P_i(z)}{n^\circ_{\,time\ step}}, \tag{2}$$

$$\mathrm{U_{av}}(z) = \sqrt[3]{\frac{\mathrm{P_{av}}(z)}{\frac{1}{2}\rho A_{layer}}}, \tag{3}$$

where A_{layer} is the frontal area of each layer along vertical direction. The computed velocity profile, site representative but synthetic, was used to run DMST for all case studies. In real applications the turbine operates in a stream velocity range limited by cut-in and cut-off speeds.

3. RESULTS ACHIEVED FOR THE CASE STUDY

We first consider results obtained without the tips losses correction. The smaller turbine ("Area 25 m^2 AR 0.67") always reaches the maximum power production per unit area (Fig. 8a). Also other configurations show good performance (Fig. 8b) even though penalized from a power production point of view, because the taller the turbine the lower the medium flow speed available.

Configuration "Area 50 m^2 AR 0.67" reaches the highest performance because of higher values of the Reynolds number since shorter turbines lead to bigger diameters and chords, so higher *Re*.

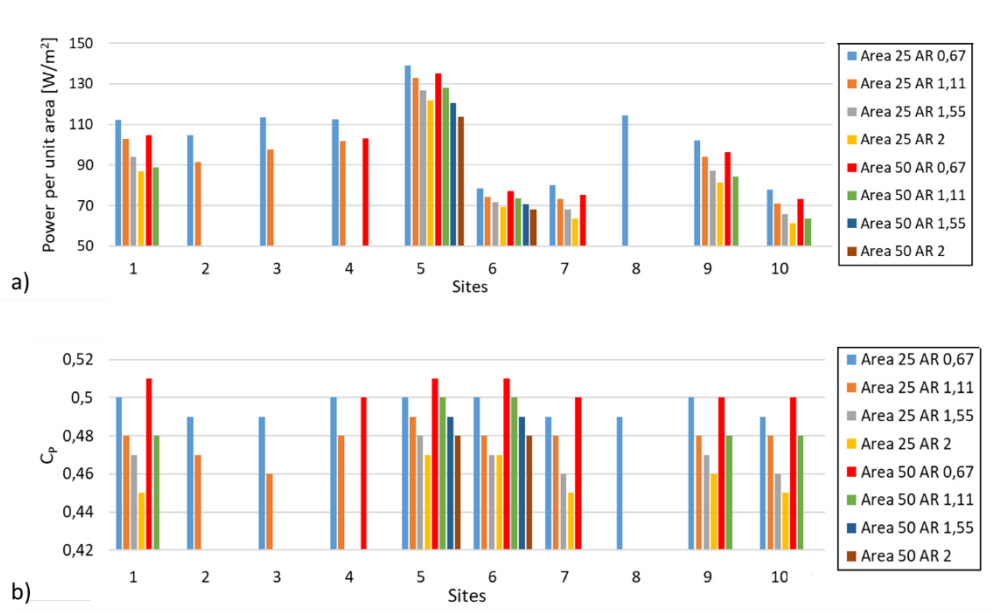

Figure 8. Comparison between different sites and different turbine geometries of a) the power per unit area production and b) performance coefficient $\boldsymbol{C_P}$ without considering tip losses.

Table 1. Maximum and minimum power per unit area value and percentage difference for each site.

Sites	1	2	3	4	5	6	7	8	9	10
P_{max}	112.3	104.5	113.4	112.3	139.2	78.4	80.0	114.5	102.2	77.8
P_{min}	86.7	91.4	97.6	101.8	113.9	68.0	63.6	114.5	81.3	61.4
Δ%	22.7	12.6	13.9	9.4	18.1	13.3	20.5	0	20.4	21.1

In Tab. 1 are summarized the maximum and minimum value of power produced per unit area and the percentage difference referred to P_{max}. It is interesting to compare sites where similar configurations are allowed, for instance in site 5 and 6 all the configurations are allowed. We see that the percentage difference in power production is higher for the first site.

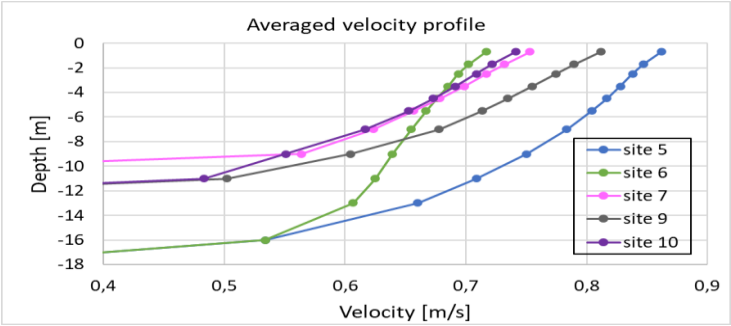

Figure 9. velocity profiles (obtained from averaged power in time) for different sites.

Looking at the velocity profile (Fig. 9) we can see that site 6 has a more rectilinear profile and the range of percentage variation of the velocity is smaller compared to the one of site 5, where the velocity profile has a more parabolic shape. Sites that have a similar percentage difference in power production, such as 7, 9 and 10 have also a similar velocity profile. In the upper part they are almost parallel, so turbines are invested by a flow with similar percentage variation of the velocity along vertical direction.

Since the vertical velocity gradient along blade causes a *TSR* variation, for each configuration we will have a unique quota where the *TSR* assumes the optimal value (i.e., giving the highest performance). Moving towards the turbine top, the *TSR* will decrease (stall condition), whereas, toward the bottom the *TSR* will increase. The choice of the operating *TSR* is fundamental to prevent a rapid deterioration of performance along the blade, especially at the blade top where the available power is high. An operating *TSR* higher than the optimal one should allow to keep high the performance at the blade top.

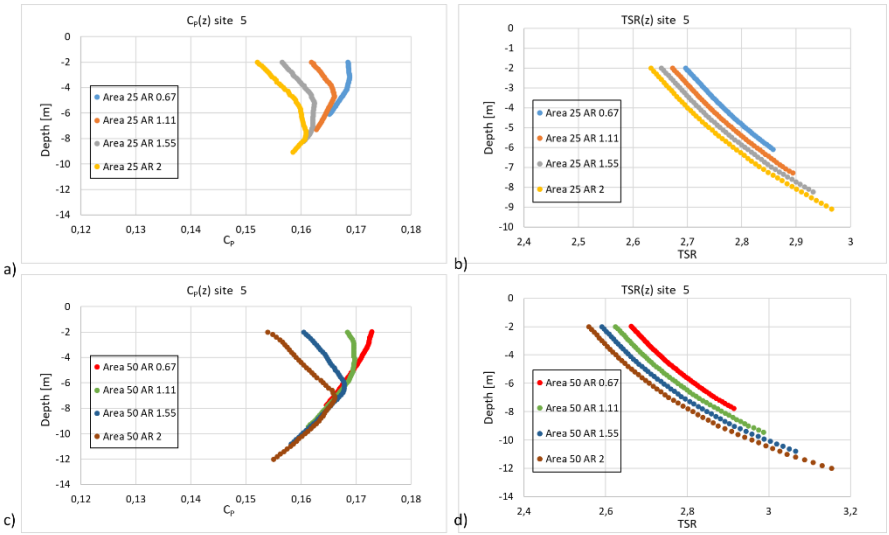

Figure 90. For frontal area of 25 m^2 C_P and *TSR* along z in a) and b) respectively and for frontal area of 50 m^2 C_P and *TSR* along z in c) and d) respectively.

Let's consider a site in particular, for instance site 5 where all the turbine configurations can be placed. Considering only turbines with frontal area equal to 25 m^2, we can see how the power coefficient varies along vertical direction as shown in Fig. 10a. Higher production (at the same *z* coordinate) is the consequence of *TSRs* closer to the optimal value. Once we have set the rotational speed for the turbine (using the operating *TSR*), the changing on flow velocity along z causes the *TSR* to vary. The maximum performance coefficient is reached at the optimum *TSR*, but it is not the same for each case, so it is reasonably *Re* dependent. Considering only turbines with frontal area equal to 50 m^2 (Fig.10 c and d) we can find again the behavior mentioned, i.e. *TSRs* closer to the optimal value lead to higher performance. Fig. 11 shows C_P and *TSR* in site 5 for all the

cases in a unique diagram and evidences how *TSR* is not the only parameter influencing performance. Indeed, the configuration "Area 25 m^2 AR 0.67" has a range of *TSR* variation smaller than the configuration "Area 50 m^2 AR 0.67", so *TSR* values are closer to the optimal value. However, the first configuration has lower performance than the second. In this case it is evident the *Re* influence. The higher the Reynolds number the higher the performance.

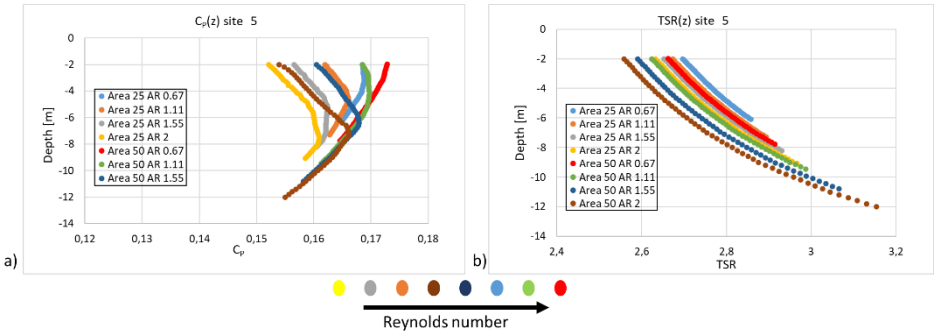

Figure 101. For all configurations in site 5 C_P and *TSR* along z respectively in a) and b). Also the Reynolds number trend for the different configurations in shown.

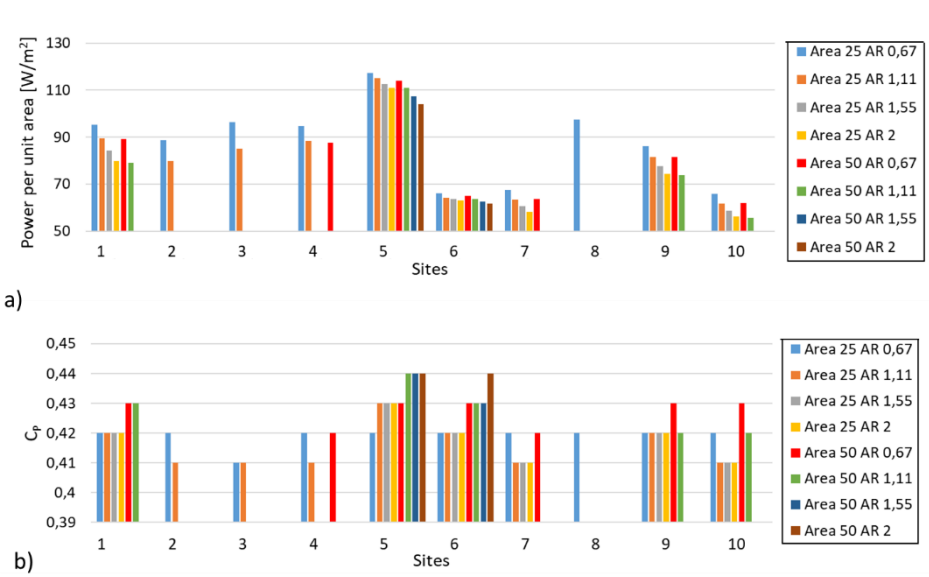

Figure 12. Comparison, between different sites and different turbine geometries, of a) the power per unit area production and b) performance coefficient C_P, considering tip losses.

Introducing tips losses, still the smaller turbine is the one with higher power production per unit area for every considered case (Fig.12). The fact that tips losses do not significantly penalize the shorter turbines, can be justified by the low σ value (for which tips losses are not crucial (Zanforlin *et al.* 2018)). The use of paired counter-rotating turbines with frontal area of 25 m^2 each, instead of a single rotor with area of 50 m^2, brings other advantages: exploit fluid dynamics mechanisms (Birjandi *et al.* 2013; Kolekar *et al.* 2015) that enhance C_P and, in case a floating platform is used to sustain the pair, the possibility to set to zero the total generator back-torque on the platform (Vergaerde *et al.* 2020) and, if the stream direction changes, to orient the platform by varying the individual torques (Kanner *et al.* 2019).

We wanted also to evaluate the suitability of the method used to estimate averaged speed profile. We carried out simulations, using all the 337 velocity profiles, for 5 significant cases. From now on we will refer to *case 1* for the one obtained with the averaged velocity profile, whereas *case 2* for the 337 simulations case. The results show that the energy production amount in both cases is quite similar. Percentage differences in energy

production (obtained as in Eq.4) are small and the gap is reasonably due to the difference of *TSR* along the blade. ΔTSR is calculated as in Eq.5.

$$\Delta energy_{\%} = \frac{Energy_{case1} - Energy_{case2}}{Energy_{case2}} * 100, \quad (4)$$

$$\Delta TSR = \frac{TSR_{bottom} - TSR_{top}}{TSR_{reference}}, \quad (5)$$

higher differences in the ΔTSR value between *case 1* and *case 2* lead to higher differences in energy production. We evaluated also the influence of the variation of the Reynolds number along the blade: from the verification (not reported for brevity) the effect is not worthy of note.

4. CONCLUSIONS

A simple methodology for site assessments, that combines a DMST routine with the flow data coming from the SHYFEM model, is described. The flow data obtained was time-averaged in terms of available kinetic power to identify 10 sites with the highest potential compatibly with bathymetric constraints, and to determine a reference vertical profile of velocity for each of them. The results, obtained by running the DMST routine with the reference velocity profile are very close to that achievable by running the routine for each one of the 337 instantaneous SHYFEM velocity profiles, proving the efficacy of the method for also energy producibility purposes and not only to compare the performance of different turbines. The results show that a pair of small CFTs gives higher power than a single CFT with the same overall frontal area, and low *AR* are more efficient than high *AR*. Both the findings can be justified by the possibility to exploit the higher flow speeds available at the top of the water column and by the more favorable distribution of *TSR* along the blade, that seem to overcome the disadvantage due to the increasing of blade tip losses entailed by the low *AR*. However, this result could be due to the low solidity of our turbine since, for very high solidity, tip losses are known to significantly penalize the C_P. The Reynolds number affect C_P at a fixed *AR*, indeed, a large frontal area allows a greater $C_P$than a small frontal area. However, this advantage cannot overtake the aforementioned benefits since, in terms of power generated per unit of frontal area, the small turbines are still preferable. This is a promising result since pair of counter-rotating CFTs are known to benefit from further C_P gains not considered in our comparative analysis. To conclude, the methodology seems sufficient to quickly identify locations with the highest hydrokinetic potential and to find the most efficient turbine aspect ratio and configuration (single or paired) taking into consideration real bathymetric constraints.

5. REFERENCES

Birjandi, A.H., Bibeau, E.L., Chatoorgoon, V. and Kumar, A. (2013). *Power measurement of hydrokinetic turbines with free-surface and blockage effect*. Ocean Engin 69:9-17.

Chougule, P. and Nielsen, S., (2014). *Overview and Design of self-acting pitch control mechanism for vertical axis wind turbine using multi body simulation approac*h. J. Phys. Conf. 524: 012055.

Deluca, S., Zanforlin, S., Rocchio, B., Haley, P.J., Foucart, C., Mirabito, C. and Lermusiaux, P.F.J. (2018). *Scalable Coupled Ocean and Water Turbine Modeling for Assessing Ocean Energy Extraction*. OCEANS 2018 MTS/IEEE Charleston, OCEAN 8604646.

Gillibrand, P., Walters, R. and McIlvenny J. (2016). *Numerical Simulations of the Effects of a Tidal Turbine Array on Near-Bed Velocity and Local Bed Shear Stress*. Energies 9:852.

Goward Brown, A.J., Neill, S.P. and Lewis, M.J. (2017). *Tidal energy extraction in three-dimensional ocean models*. Renewable Energy 114:244-257.

Kanner, S., Koukina, E. and Yeung, R.W. (2019). *Power optimization of model-scale floating wind turbines using real-time hybrid testing with autonomous actuation and control*. J. Offshore Mech. Arct. Eng. June 2019, 141(3): 031902.

Kinzel, M., Mulligan, Q. and Dabiri, J.O. (2012). *Energy exchange in an array of vertical-axis wind turbines*. Journal of Turbulence, 13:1-13.

Kolekar, N and Banerjee, A. (2015). *Performance characterization and placement of a marine hydrokinetic turbine in a tidal channel under boundary proximity and blockage effects*. Applied Energy 148:121-133.

Migliore, P.G., Wolfe, W.P. and Fanucci, J.B. (1980). *Flow Curvature Effects on Darrieus Turbine Blade Aerodynamics*, J. Energy 4:49–55.

Orlandi, A., Collu, M., Zanforlin, S. and Shires, A., (2015). *3D URANS analysis of a vertical axis wind turbine in skewed flows*. J Wind Eng Ind Aerodyn 147:77-84.

Paraschivoiu, I. (2002). *Wind Turbine Design with Emphasis on Darrieus Concept*, Polytechnic International. *Press*

Pucci, M., Zanforlin, S., Bellafiore, D. and Umgiesser, G. (2020). *Embedding of a Blade-Element Analytical Model into the SHYFEM Marine Circulation Code to Predict the Performance of Cross-Flow Turbines*. Journal of Marine Science and Engin., 8(12):1–21, 1010.

Ramírez-Mendoza, R., Murdoch, L., Jordan, L., Amoudry, L., McLelland, S., Cooke, R., Thorne, P., Simmons, S., Parsons, D. and Vezza, M. (2020). *Asymmetric effects of a modelled tidal turbine on the flow and seabed*. Renew. Energy 159:238–249.

Rocchio, B., Chicchiero, C., Salvetti, M.V. and Zanforlin, S. (2020). *A simple model for deep dynamic stall conditions*. Wind Energy 23(4):915-938.

Shen, W.Z., Mikkelsen, R. and Sorensen J.N. (2005). *Tip Loss Corrections for Wind turbine Computations.* Wind Energy 8:457-475.

Thiébot, J., Guillou, N., Guillou, S., Good, A. and Lewis, M. (2020). *Wake field study of tidal turbines under realistic flow conditions*. Renew. Energy 151:1196–1208.

Umgiesser, G., Ferrarin, C., Fivan, Bajo, M. SHYFEM-Model/Shyfem: Stable Release 7.4.1; Version VERS_7_4_1; Zenodo: Meyrin, Switzerland, 2018; Available online: http://doi.org/10.5281/zenodo.1311751 (accessed on 13 July 2018).

Vergaerde, A., De Troyer, T., Muggiasca, S., Bayati, I., Belloli, M., Kluczewska-Bordier, J., Parneix, N., Silvert, S. and Runacres, M.C. (2020). *Experimental characterization of the wake behind paired vertical-axis wind turbines*, J. Wind Engin. & Industrial Aerodyn. 206:104353.

Zanforlin, S. (2018) *Advantages of vertical axis tidal turbines set in close proximity: A comparative CFD investigation in the English Channel*. Ocean Engineering 156:358-372.

Zanforlin, S. and Deluca, S. (2018). *Effects of the Reynolds number and the tip losses on the optimal aspect ratio of straight-bladed Vertical Axis Wind Turbines.* Energy 148 179-195.